Effect of pairing on one- and two-nucleon transfer below the Coulomb barrier: A time-dependent microscopic description

Guillaume Scamps* and Denis Lacroix†
GANIL, CEA/DSM and CNRS/IN2P3, Boîte Postale 55027, 14076 Caen Cedex, France
(Received 30 November 2012; published 10 January 2013)

The effect of pairing correlation on transfer reaction below the Coulomb barrier is investigated qualitatively and quantitatively using a simplified version of the time-dependent Hartree-Fock + BCS approach. The effect of particle-number symmetry breaking on the description of reaction and dedicated methods to extract one- and two-nucleon transfer probabilities (P_{1n} and P_{2n}) in a particle-number symmetry breaking approach are discussed. The influence of pairing is systematically investigated in the ^{40}Ca + ^{40,42,44,46,48,50}Ca reactions. A strong enhancement of the two-particle transfer probabilities owing to initial pairing correlations is observed. This enhancement induces an increase of the ratio of probabilities $P_{2n}/(P_{1n})^2$ compared to the case with no pairing. It is shown that this ratio increases strongly as the center-of-mass energy decreases with a value that could be larger than ten in the deep sub-barrier regime. An analysis of the pair transfer sensitivity to the type of pairing interaction, namely surface, mixed, or volume, used in the theory is made. It is found that the pair transfer is globally insensitive to the type of force and depends mainly on the pairing interaction strength.

DOI: 10.1103/PhysRevC.87.014605 PACS number(s): 25.40.Hs, 21.10.Pc, 21.60.Jz, 27.60.+j

I. INTRODUCTION

The possibility to access a cross section much below the Coulomb barrier has revealed new aspects, such as the hindrance of fusion cross section (see, for instance, Ref. [1]), whose origin is still debated [2,3]. Among possible interpretations, other competing processes such as single- or multinucleon transfer might eventually be enhanced and/or modify the capture process [4,5]. New experimental observations [6–8] in the moderate and deep sub-barrier regime might lead to important new insight, especially into the process of pair transfer. The description of such pair transfer is particularly complex because it requires to treat the quantum tunneling of a composite, eventually correlated, system. In particular, pairing correlations among last bound nucleons are anticipated to play a crucial role. Following the pioneering work of Refs. [9–12], an important effort is currently being made to improve the description of pair transfer in superfluid systems [13–23]. These approaches usually have in common that transition probabilities from the initial to the final nucleus are estimated using state-of-the-art Hartree-Fock Bogolyubov (HFB) and quasiparticle random phase approximation (QRPA) nuclear models while the reaction-dynamics part is treated in completely separated steps using coupled-channels technique.

The present work is an attempt to treat nuclear structure and nuclear reaction aspects in a common microscopic framework that includes pairing. Recently, active research has been devoted to include pairing correlations into the nuclear dynamics using the time-dependent HFB (TDHFB) approach [15,24,25]. While current applications can be performed in an unrestricted space, owing to the required effort, applications of TDHFB have been essentially made on processes involving one nucleus, such as giant resonances. The use of TDHFB to nuclear reactions remains tedious. A simplified version of TDHFB based on the BCS approximation is considered. This theory was proposed some time ago [26] and recently applied with some success to both collective motion in nuclei [27] and reactions in 1D models [28]. First step toward collisions was reported in Ref. [29]. The TDHF + BCS approach has the advantage of being simpler than the original TDHFB theory while keeping part of the physics of pairing. Note that time-dependent microscopic theories have several advantages compared to other techniques. Many effects, such as possible dynamical deformation or core polarization during the reaction, are automatically accounted for. In addition, other competing phenomena such as emission to the continuum and/or fusion are simultaneously treated. Because many aspects of the theory applied here have been extensively discussed in Refs. [27,28], only the main-aspect features are recalled below.

II. NUCLEAR REACTIONS WITH PAIRING

Time-dependent Hartree-Fock (TDHF) has become a standard tool to describe nuclear reactions such as fusion or transfer reactions (see Ref. [30] and references therein). In the present work, the TDHF3D code of Ref. [31] is extended to include pairing correlations. Below, specific aspects related to the introduction of pairing are discussed.

A. Initial conditions

The reaction is simulated on a three-dimensional mesh. Following the standard procedure [31], the two nuclei are initiated separately and then positioned consistently with the desired impact parameter b and center-of-mass energy $E_{\text{c.m.}}$. The initial wave function can be written as

$$|\Psi(t_0)\rangle = |\Phi_1(t_0)\rangle \otimes |\Phi_2(t_0)\rangle, \quad (1)$$

*scamps@ganil.fr
†lacroix@ganil.fr

where $|\Phi_\alpha(t_0)\rangle$ denotes the many-body wave function of nucleus $\alpha = 1, 2$. Usually, these wave functions correspond to Slater determinants. It is assumed here to take the more general form of a quasiparticle vacuum written as

$$|\Phi_\alpha(t_0)\rangle = \prod_{k>0} \left[u_k^\alpha(t_0) + v_k^\alpha(t_0) a_k^\dagger(t_0) a_{\bar{k}}^\dagger(t_0)\right]|-\rangle, \quad (2)$$

where $a_k^\dagger(t_0)$ stands for the creation operator associated with the canonical single-particle states, denoted hereafter by $|\varphi_k(t_0)\rangle$, while $[u_k(t_0), v_k(t_0)]$ are the standard upper and lower components of the quasiparticle states. Note that owing to the spatial separation of the two nuclei, a common single-particle basis can be used. Accordingly, we can omit the α index and directly write the total wave function as

$$|\Psi(t_0)\rangle = \prod_{k>0} [u_k(t_0) + v_k(t_0) a_k^\dagger(t_0) a_{\bar{k}}^\dagger(t_0)]|-\rangle. \quad (3)$$

In practice, initial states for each nucleus have been obtained using the EV8 code [32] that solves the self-consistent BCS equations in the energy density functional framework [33]. Single-particle states are written in $\mathbf{r}$ space and spin space, denoted by $\sigma = \uparrow, \downarrow$ as

$$a_k^\dagger = \sum_\sigma \int d\mathbf{r} \varphi_k(\mathbf{r}, \sigma) \Psi_\sigma^\dagger(\mathbf{r}), \quad (4)$$

where $\Psi_\sigma^\dagger(\mathbf{r})$ are standard spinors creation operators. In EV8, time-reversal symmetry is assumed and single-particle states can be grouped by pairs of time-reversed states $(k, \bar{k})$. Associated quasiparticle creation operators $(\beta_k^\dagger, \beta_{\bar{k}}^\dagger)$ are written using the following convention for the Bogolyubov transformation:

$$\begin{cases} \beta_k^\dagger = \sum_{\mathbf{r}} u_k(\mathbf{r}, t_0) \Psi_\uparrow^\dagger(\mathbf{r}) + v_k(\mathbf{r}, t_0) \Psi_\downarrow(\mathbf{r}), \\ \beta_{\bar{k}}^\dagger = \sum_{\mathbf{r}} u_k(\mathbf{r}, t_0) \Psi_\downarrow^\dagger(\mathbf{r}) - v_k(\mathbf{r}, t_0) \Psi_\uparrow(\mathbf{r}), \end{cases} \quad (5)$$

where, using time-reversal properties, we have

$$u_k(\mathbf{r}, t_0) = u_k \varphi_{\bar{k}}(\mathbf{r}, \uparrow) = u_k \varphi_k(\mathbf{r}, \downarrow), \quad (6)$$

$$v_k(\mathbf{r}, t_0) = v_k \varphi_k^*(\mathbf{r}, \downarrow) = v_k \varphi_{\bar{k}}^*(\mathbf{r}, \uparrow). \quad (7)$$

The Skyrme Sly4d functional [31] is used in the mean-field channel while for pairing, the following effective neutron-neutron interaction is used:

$$V_\tau(\mathbf{r}, \sigma; \mathbf{r}', \sigma') = V_0^{\tau\tau} \left(1 - \eta \frac{\rho([\mathbf{r} + \mathbf{r}']/2)}{\rho_0}\right) \delta_{\mathbf{r},\mathbf{r}'} [1 - P_{\sigma\sigma'}],$$

where $P_{\sigma\sigma'}$ is the spin exchange operator and where $\rho_0 = 0.16$ fm^{-3}. Here $\tau = n, p$ stands for neutron or proton channel; only neutron-neutron and proton-proton interaction are considered. Three different forces, standardly called volume ($\eta = 0$), mixed ($\eta = 0.5$), and surface ($\eta = 1$), are used below. In each case, the neutron pairing interaction strength V_0^{nn} was adjusted to properly reproduce the experimental gap for the calcium isotopic chain deduced from masses using the five-points formula [34]. Theoretical odd systems binding energies have been computed using blocking techniques. Values of the interaction parameters are reported in Table I. The proton interaction strength is taken from Ref. [35] but do not play any role owing to the proton closed shell. Illustrations of the pairing gap obtained for the three results of the fit are shown in Fig. 1 for the three types of pairing interaction. A comparison of the neutron pairing gap $\Delta_n^{(5)}$ obtained using the different interactions is shown in Fig. 1. The three interactions lead to gaps that are compatible with each others and compatible with the experimental gaps along the calcium isotopic chains especially in the midshell. In the following, we consider systematically reactions between the doubly magic ^{40}Ca nucleus and other ^{4x}Ca isotopes. The two reactions $^{40}\text{Ca} + ^{40}\text{Ca}$ and $^{40}\text{Ca} + ^{48}\text{Ca}$ correspond to reactions between two normal systems, while in other cases, one of the nuclei presents pairing.

TABLE I. Parameters of the neutron-neutron and proton-proton pairing strength used in the present work.

Interaction	η	V_0^{nn} (MeV fm^3)	V_0^{pp} (MeV fm^3)
Volume	0	585	490
Mixed	0.5	798	755
Surface	1	1256	1462

B. Time-dependent equation of motion

Once the two nuclei have been initiated, the reaction is simulated by performing the dynamical evolution of the many-body wave packet given by Eq. (3). Here, the TDHF + BCS approximation that may be derived from a variational principle [26] or by an approximate reduction of the TDHFB equations [27] is used. Because properties as well as numerical aspects of the TDHF + BCS method are discussed in Refs. [27,28], only the main ingredients of the theory are summarized here. In this theory, the wave function remains at all times in its canonical basis [Eq. (3)] and the single-particle states' evolution identifies with the mean-field dynamics with

$$i\hbar \partial_t |\varphi_k\rangle = (h[\rho] - \eta_k)|\varphi_k\rangle, \quad (8)$$

where $\eta_k(t) = \langle\varphi_k(t)|h[\rho]|\varphi_k(t)\rangle$ is a time-dependent phase that is conveniently chosen to minimize the effect of the U(1) symmetry breaking. $h[\rho]$ corresponds here to the self-

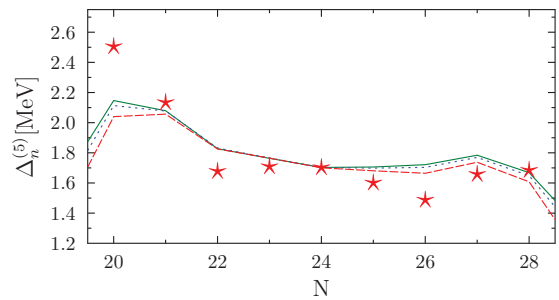

FIG. 1. (Color online) Experimental (red stars) and theoretical neutron gaps for $Z = 20$ as a function of N. The volume, mixed, and surface interactions are respectively shown by solid, dotted, and dashed lines.

consistent mean field derived from the Skyrme functional including time-odd components.

Along the dynamical path, the information is contained in the normal and anomalous densities, denoted by ρ and κ written in $\mathbf{r}$ space as

$$\rho_{\sigma\sigma'}(\mathbf{r},\mathbf{r}') = \sum_{k\gtrless 0} n_k \varphi_k^*(\mathbf{r},\sigma)\varphi_k(\mathbf{r}',\sigma'), \tag{9}$$

$$\kappa_{\sigma\sigma'}(\mathbf{r},\mathbf{r}') = \sum_{k>0} \kappa_k [\varphi_k(\mathbf{r},\sigma)\varphi_{\bar{k}}(\mathbf{r}',\sigma') - \varphi_{\bar{k}}(\mathbf{r},\sigma)\varphi_k(\mathbf{r}',\sigma')]. \tag{10}$$

$(k,\bar{k})$ corresponds to pair of single-particle states that were originally degenerated in the static calculation owing to time-reversal symmetry. $n_k = v_k^2$ denote the occupation numbers while $\kappa_k = u_k^* v_k$ are the components of the anomalous density in the canonical basis. Conjointly to the single-particle evolution, the equation of motion of the components (u_k, v_k) or equivalently of (n_k, κ_k) should be specified. Following Ref. [27], we have

$$\begin{aligned} i\hbar\frac{d}{dt}n_k(t) &= \kappa_k(t)\Delta_k^*(t) - \kappa_k^*(t)\Delta_k(t), \\ i\hbar\frac{d}{dt}\kappa_k(t) &= \kappa_k(t)[\eta_k(t) + \eta_{\bar{k}}(t)] + \Delta_k(t)[2n_k(t) - 1], \end{aligned} \tag{11}$$

where $\Delta_k(t)$ correspond to the pairing field components given by

$$\Delta_k(t) = -\sum_{l>0} \overline{v}_{k\bar{k}l\bar{l}}\kappa_l(t)g_l(t). \tag{12}$$

g_k corresponds to the cutoff function that selects the pairing window. This cutoff should be taken consistently with the static calculation [32]. Here, a slightly different prescription is used compared to the original EV8 with

$$g_k(t) = f[\eta_k(t) - \lambda]f[\lambda - \eta_k(t)]\theta[-\eta_k(t)]. \tag{13}$$

f here corresponds to a Fermi distribution with a cutoff at 5 MeV and a stiffness parameter equal to 0.5 MeV [32], while $\theta(\eta)$ equals one for $\eta > 0$ and zero elsewhere. This additional cutoff ensures that only states that are initially bound are considered during the evolution.

As discussed in Ref. [28], the reduction of the TDHFB to TDHF + BCS leads to some inconsistencies, especially regarding the one-body continuity equation, making the interpretation of the dynamics difficult. To avoid this problem, we used here the frozen occupation approximation (FOA). In the FOA, it is assumed that the main effect of pairing originates from the initial correlations that induce partial occupations of the orbitals and nonzero components of the two-body correlation matrix, denoted by C_{12}. Possible reorganization in time of occupation numbers and components of C_{12} are neglected. Said differently, occupation numbers n_k and components κ_k are kept fixed in time and equal to their initial values. Note that similar ideas have been used recently to describe two-particle break-up reaction using the time-dependent density-matrix approach [36]. This simplification is motivated by the fact that (i) it solves the problem of the continuity equation [28]; (ii) in the simple one-dimensional model considered in the same reference, it gives rather good description of the emission of particles and is sometimes more predictive than the full TDHFB theory; and (iii) the FOA approximation applied to collective motion in nuclei [37] gives results that are very close to the full TDHF + BCS dynamics reported in Ref. [27].

C. Illustration of reactions

In the present work, we are interested in reactions below the Fusion barrier such as the one presented in Ref. [7], where the probabilities to transfer x neutrons, denoted by P_{xn} can be extracted as a function of the minimal distance of approach D during the collision. Assuming a Coulomb trajectory, D is related to the center-of-mass energy $E_{\text{c.m.}}$ through

$$D = \frac{Z_P Z_T e^2}{2E_{\text{c.m.}}}\left[1 + \frac{1}{\sin(\theta_{\text{c.m.}}/2)}\right], \tag{14}$$

where Z_P and Z_T are the target and projectile proton number, while $\theta_{\text{c.m.}}$ is the center-of-mass scattering angle. Following Ref. [38], only central collisions are considered here and different distances D are simulated by varying the center-of-mass energy. Initial conditions are obtained on a lattice of $2L_x \times 2L_y \times 2L_z = 22.4 \times 22.4 \times 22.4$ fm^3 noting that the EV8 code uses symmetries to reduce the calculation in one octant of this space. The dynamical evolutions are performed in the center-of-mass frame using a Runge-Kutta 4 algorithm on a spatial grid of $L_x \times L_y \times 2L_z = 60.8 \times 22.4 \times 22.4$ fm^3 with a lattice spacing $\Delta x = 0.8$ fm. The time step is $\Delta t = 0.015 \times 10^{-22}$ s. Note that nonequilibrium particle emission is negligible owing to the small center-of-mass energy in the entrance channel.

As an illustration, the neutron density profiles of the reaction ^{46}Ca + ^{40}Ca are shown at different stages of the reaction in Fig. 2. During the reaction, the two nuclei approach each other, stick together during a certain time, and then reseparate. During the contact time that strongly depends on the initial center-of-mass energy, they eventually exchange particles.

D. Particle transfer probability in normal systems

In practice, the system can be cut into two pieces at the neck position to calculate the expectation value of the number of exchanged nucleons from one side to the other. By convention, we denote by B the subspace where the lightest nucleus is initially (to the right of the neck position in Fig. 2) and by $\bar{B}$ the rest of the total space. In a mean-field approach, the simplest way to obtain the number of exchanged particles is to estimate the operator $\hat{N}_B$ defined through [39]

$$\hat{N}_B = \sum_\sigma \int d\mathbf{r}\Psi_\sigma^\dagger(\mathbf{r})\Psi_\sigma(\mathbf{r})\Theta(\mathbf{r}), \tag{15}$$

with the time-dependent wave function (3). Here $\Theta(\mathbf{r})$ is zero on the left side of the neck and 1 elsewhere.

An illustration of the mean number of transferred particles, denoted by $N_{\text{tr}} \equiv \langle\hat{N}_B\rangle - 20$, from ^{46}Ca to ^{40}Ca at center-of-mass energy $E_{\text{c.m.}} = 49$ MeV is shown in Fig. 3 (solid line). As discussed in Ref. [38], a deeper understanding of the transfer process can be achieved by introducing projection onto good

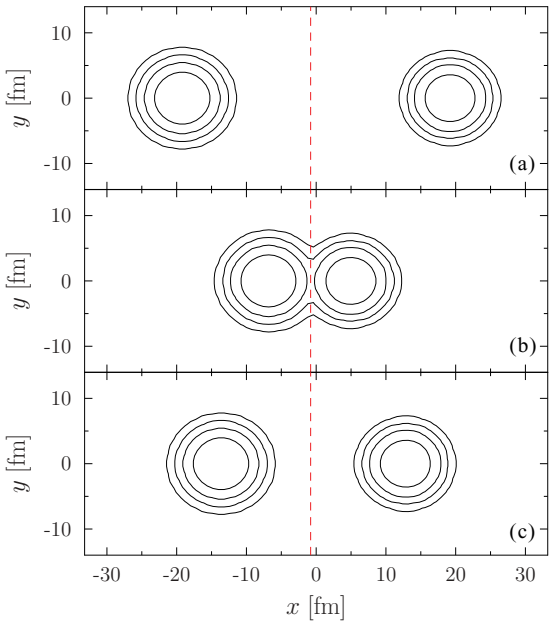

FIG. 2. (Color online) Evolution of the neutron density projected onto the reaction plane $z = 0$, for the reaction ^{46}Ca + ^{40}Ca at impact parameter $b = 0$ fm and center-of-mass energy $E_{\text{c.m.}} = 49$ MeV at initial time (a), $t = 20 \times 10^{-22}$ s (b), and $t = 37 \times 10^{-22}$ s (c). The neck position is indicated by the dashed vertical line.

particle numbers in the subspace B (or equivalently $\bar{B}$). The projection operator on a given number of particles N inside the subspace B can be written as (see Ref. [38])

$$\hat{P}_B(N) = \frac{1}{2\pi}\int_0^{2\pi} d\varphi e^{i\varphi(\hat{N}_B - N)}, \tag{16}$$

where φ is the standard gauge angle. Then the probability to find N particles in the subspace B is

$$\begin{aligned} P_B(N) &= \langle\Psi(t)|\hat{P}_B(N)|\Psi(t)\rangle \\ &= \frac{1}{2\pi}\int_0^{2\pi} d\varphi e^{-i\varphi N}\langle\Psi(t)|\Psi_B(\varphi,t)\rangle, \end{aligned} \tag{17}$$

where $|\Psi_B(\varphi,t)\rangle = e^{i\varphi\hat{N}_B}|\Psi(t)\rangle$ is a new quasiparticle vacuum obtained from the original one by making a rotation φ in the gauge space from the original state.

The probabilities extracted by projection are linked to the mean number of particles through the sum rule:

$$\langle\hat{N}_B\rangle = \sum_N N P_B(N). \tag{18}$$

Usually, experimental data are presented in terms of probabilities to exchange $1, 2, \ldots, x$ neutrons (resp. protons), denoted respectively by $P_{1n}, P_{2n}, \ldots, P_{xn}$ (respectively, $P_{1p}, P_{2p}, \ldots, P_{xp}$). In the present reaction, these probabilities are defined through $P_{xn} = P_B(20 + x)$, while the above sum rule reads $N_{\text{tr}} = \sum_x x P_{xn}$.

In the present work, probabilities have been evaluated using the Pfaffian technique of Ref. [40] and explicit formulas for the wave packet are given in the Appendix . An illustration of P_{1n} and P_{2n} probabilities obtained using the projection method is shown in panel (a) of Fig. 3 for ^{46}Ca. As already noted

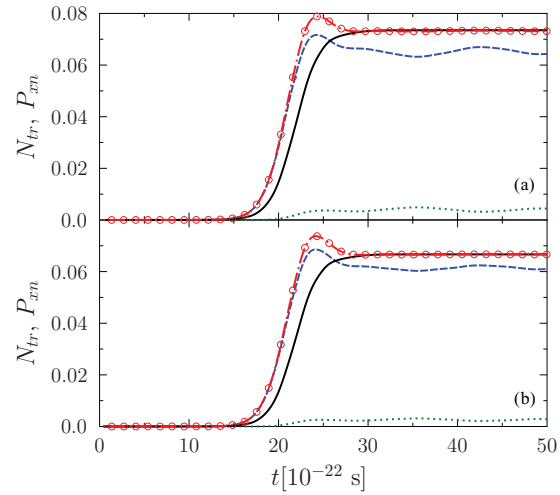

FIG. 3. (Color online) Evolution of the mean number of particles transferred from ^{46}Ca to ^{40}Ca as a function of time during the reaction illustrated in Fig. 2. The probability P_{1n} (dashed line) and P_{2n} (dotted line) to exchange 1 and 2 particles obtained by making projection on the side B are also presented as well as the quantity $P_{1n} + 2P_{2n}$ (open circles). (a) Mean number of particles and probabilities obtained without projecting on good particle number in the total space. (b) Same with an additional projection on neutron number $N = 46$ in the total space.

in Ref. [38], the $1n$ and $2n$ channels are often dominating over other multinucleon transfer channels leading to $N_{\text{tr}} \simeq P_{1n} + 2P_{2n}$, which is perfectly fulfilled in Fig. 3 after the two nuclei reseparate.

E. Particle transfer probability in superfluid systems

Strictly speaking, the above method to extract transfer probabilities is valid only for normal systems, i.e., when the wave function (3) identifies with a Slater determinant that is an eigenstate of particle number. For nuclei that present pairing, the initial wave function explicitly breaks the particle number symmetry and the BCS states are obtained by imposing the particle number only on average. This is, for instance, the case for the ^{46}Ca discussed above. Said differently, the ground state that is used for ^{46}Ca not only presents a component with $N = 26$ neutrons but also with the surrounding number of neutrons. These components lead to spurious contributions in the probabilities extracted in previous section. A possible way to remove this contamination is to first select the relevant component with $N_0 = 20 + 26$ particles in the full space and then consider the projection onto different particle numbers in the subspace B. In the following, we denote by $\hat{P}(N_0)$ the projector on N_0 particles in the full space,

$$\hat{P}(N_0) = \frac{1}{2\pi}\int_0^{2\pi} d\varphi e^{i\varphi(\hat{N} - N_0)}, \tag{19}$$

where $\hat{N}$ is now the complete particle-number operator. More generally, to estimate the possible effect of contribution from components $N \neq N_0$, one can compute the probability $P(N)$ that the initial state belongs to the Hilbert space of N particles.

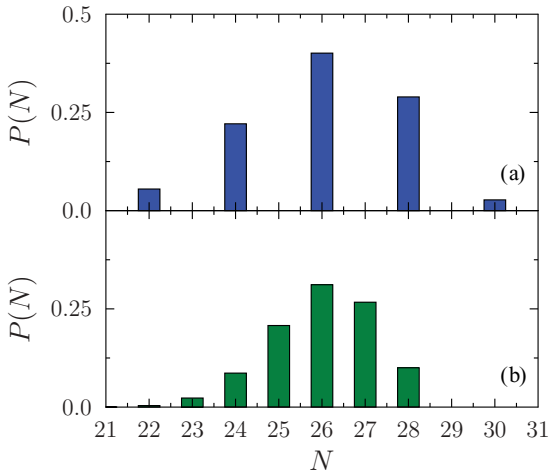

FIG. 4. (Color online) Illustration of the distribution of probabilities to have N particles initially for the ^{40}Ca + ^{46}Ca reaction in the TDHF + BCS case (a) and TDHF with initial filling approximation (b). Note that because ^{40}Ca has a good particle number, N is defined here as the number of particles in the wave function describing the ^{46}Ca and is centered around $N = 26$.

This probability is defined through

$$P(N) = \langle \Psi(t_0)|\hat{P}(N)|\Psi(t_0)\rangle \tag{20}$$

and is shown in Fig. 4(a). Because ^{40}Ca has a well-defined number of particles, by convention, N in the x axis of Fig. 4 is taken here as the number of particles of its collision partner. Only even components are nonzero owing to the specific form of the state [Eq. (3)]. While the distribution is properly centered around the imposed mean number of particles, non-negligible contributions coexist, especially for $N = N_0 \pm 2$ in the initial state.

To remove possible influence of these spurious components, it is possible to define at all times a state with a good number of neutrons,

$$|N_0(t)\rangle \equiv \frac{1}{\sqrt{\langle \Psi(t)|\hat{P}(N_0)|\Psi(t)\rangle}}\hat{P}(N_0)|\Psi(t)\rangle. \tag{21}$$

Then, the mean number of transferred particle as well as probabilities P_{xn} can be computed using the same technique as in Sec. II D. Note that the double-projection approach proposed here can be regarded as a first step towards the projection after variation (PAV) approach standardly applied in nuclear structures, generalized here to binary reactions. An illustration of the result is given in panel (b) of Fig. 3. The comparison of the projected (b) and unprojected (a) panels show that $N_{\rm tr}$ and P_{1n} are only slightly affected by the removal of spurious components. This is a quite general feature we observed in applications presented in the article. However, the difference between P_{2n} with and without projection can be as large as several orders of magnitude. This conclusion also holds for a larger number of particles transferred.

A second difficulty arises, which could already be seen in Fig. 3, when pairing is nonzero. While $N_{\rm tr}$ after collisions converges to a well-defined asymptotic value, small oscillations of P_{1n} and P_{2n} around their asymptotic values remain. These

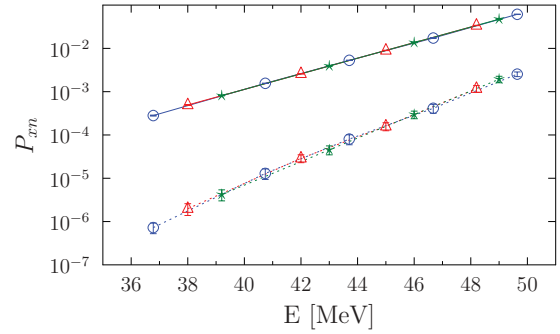

FIG. 5. (Color online) Comparison of asymptotic probabilities P_{1n} (solid line) and P_{2n} (dotted line) obtained with the three pairing interactions for the ^{40}Ca + ^{46}Ca at various center-of-mass energies below the fusion barrier: volume (open circles), mixed (open triangles), and surface (stars) interactions. Note that error bars owing to final time oscillations are also presented but are very small.

oscillations are also present if the expectation value $\langle \hat{N}_B^2 \rangle$ is computed as a function of time with or without projection onto good particle number in the total space. This problem points out a difficulty in theories such as TDHF + BCS. In a previous article [28], we showed that the one-body continuity equation is always respected in TDHFB, while in TDHF + BCS, it is respected only if single-particle occupations are frozen, which is the case in the present work. However, these theories provide only approximate treatment of the two-body density matrix and, in particular, do not respect the two-body continuity equation. This difficulty is not specific to the TDHF + BCS theory but is also present in TDHFB. Indeed, we have checked in the 1D model developed in Ref. [28], adapted to treat transfer, that similar oscillations occur even if the full TDHFB is solved. In the following, results obtained for nuclei with nonvanishing pairing are presented with error bars with height equal to oscillation amplitudes. In most cases displayed below, error bars are too small to be seen.

F. Sensitivity to the pairing residual interaction

Three different pairing interactions, presented in Sec. II A, have been used to initialize the collision partners. These interactions lead to different spatial properties of the pairing field but have been adjusted to reproduce the experimental gaps (see Fig. 1). In Fig. 5, asymptotic values of one- and two-nucleon transfer probabilities are reported as a function of center-of-mass energy for the ^{40}Ca + ^{46}Ca for the three pairing interactions below the Fusion barrier. As seen in the figure, the extracted transfer probabilities are insensitive to the type of interaction used. It turns out that whatever is the form of the pairing effective zero-range vertex, if the interaction is carefully adjusted to reproduce the same experimental gap (Fig. 1), the final transfer rate is also the same. Note that the present finding is not in contradiction with Ref. [22], where different types of interactions (mixed and surface) were shown to give different two-particle transfer from ground state to ground state. The two forces used in Ref. [22] have been adjusted to reproduce the same two neutron separation energies but lead to different pairing gaps. In the present work, we do not

see any evidence of a dependence of the pair transfer process on the shape of the pairing force that is used.

Because all types of force lead to the same probabilities, below only results of one of the interaction (mixed) are shown.

G. The no-pairing limit

Here, we are interested in the enhancement of pair transfer probabilities as the pairing is introduced in the transport theory. To quantify this enhancement, it is necessary to also perform calculation without pairing interaction, i.e., TDHF. An additional difficulty arises in the comparison between systems with and without pairing. Quite often, especially when a given j shell is partially occupied, nuclei initialized with EV8 in the Hartree-Fock limit are deformed. The introduction of pairing stabilizes the spherical shape. Therefore, a direct comparison of the case with and without pairing not only probes the effect of pairing but also the effect of deformation that is (i) not correct for calcium isotopes (ii) not the objective of the present work.

To avoid, possible effects of deformation, we used the filling approximation for the last occupied shell; i.e., we assume that the last shell has partial occupations n_k such that all angular momentum projections m are occupied in the same way. This ensures the convergence of the mean-field theory towards nondeformed systems. This approach implies that the initial system is not anymore described by a wave packet like in Eq. (3), which would identify with a Slater determinant in the usual TDHF, but by a many-body density matrix of the form

$$\hat{D}(t) = \frac{1}{Z}\exp\left[-\sum_k \lambda_k a_k^\dagger(t)a_k(t)\right], \qquad (22)$$

where $Z = \mathrm{Tr}\{\exp[-\sum_k \lambda_k a_k^\dagger(t)a_k(t)]\}$. The trace here is taken on the complete Fock space, while $a_k^\dagger(t)$ corresponds to creation operator of the canonical states $\varphi_k(t)$. In the filling approximation, the density operator corresponds to a statistical density and the information on the system reduces to the knowledge of the one-body density matrix $\rho = \sum_k |\varphi_k(t)\rangle n_k \langle\varphi_k(t)|$, where the occupation numbers are related to the coefficients through $n_k = 1/(1+e^{\lambda_k})$. The evolution of $\hat{D}(t)$ is performed by generalizing the TDHF approach where the single-particle states evolve according to the standard self-consistent equation of motion [Eq. (8)] while the occupation numbers are kept fixed in time. As far as we know, this is the only way to avoid possible mixing of deformation and pairing effects and this procedure is taken below as the no-pairing reference.

Similar to the pairing case, for non-doubly magic nuclei, the density $\hat{D}(t)$ mixes systems with different particle numbers and similar treatment based on double projections is necessary to extract transfer probabilities. In the Appendix, some helpful formulas to perform projection on statistical densities of the form [Eq. (22)] are given. An illustration of the decomposition of the initial state with a mean neutron number $\langle N\rangle = 26$ corresponding to the ^{46}Ca is given in panel (b) of Fig. 4. This figure illustrates that the width of the distribution is comparable

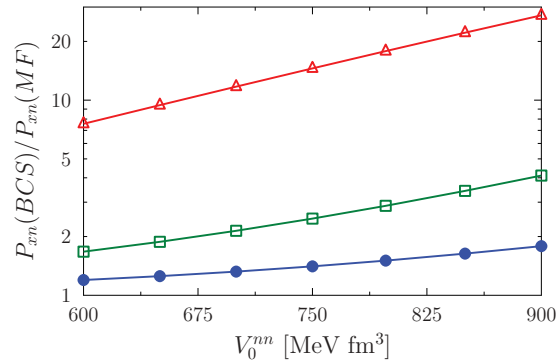

FIG. 6. (Color online) Ratio of probabilities P_{xn}(BCS)/P_{xn}(MF) as a function of the pairing strength interaction V_0^{nn} for the reaction ^{40}Ca + ^{46}Ca at $E_{\mathrm{c.m.}} = 43.7$ MeV. P_{1n}(BCS)/P_{1n}(MF) (solid circles) and P_{2n}(BCS)/P_{2n}(MF) calculated by neglecting (open squares) or not (open triangles) the anomalous density components are shown.

to the BCS case (a) with the difference that odd components are also present in the filling approximation. Probabilities obtained with the filling approximation are labeled by P_{xn}(MF) while those with pairing are labeled by P_{xn}(BCS).

As a first illustration of the enhancement of pair transfer probabilities when pairing is introduced, we have extracted systematically the ratios between probabilities with and without pairing as the pairing interaction strength V_0^{nn} is varied in the mixed interaction for the reaction ^{40}Ca + ^{46}Ca at $E_{\mathrm{c.m.}} =$ 43.7 MeV. These ratios are shown in Fig. 6 as a function of V_0^{nn}. When pairing is accounted for, the two nucleons probabilities have been computed using either nonzero components of the anomalous density (open triangles) or neglecting them (open squares). While the former case corresponds to the appropriate treatment of pairing effects, the latter case can be regarded as a reference calculation where only the sequential transfer of the two neutrons is treated while taking properly the occupation number dispersion of single-particle states around the Fermi energy. The pairing correlations strongly enhanced the two-particle transfer, by an order of magnitude around the physical value of the pairing strength (see Table I). Note that the enhancement depends on the energy of the collision (see below). A smaller but nonzero effect is also seen in the one-particle transfer channel. The small increase in P_{1n} stems from the increase of occupation number fragmentation as V_0^{nn} increases. The strong enhancement observed when the anomalous density is not neglected compared to the case where it is set to zero clearly shows that the increase is interpreted as the contribution from direct simultaneous processes.

III. RESULTS AND DISCUSSION

In the present work, we have systematically investigated the effect of initial pairing correlations on the single- and multinucleon transfer by comparing the TDHF + BCS with frozen correlations to the mean-field dynamics with the filling approximation for collision between a ^{40}Ca and different calcium isotopes below the Fusion barrier. In Table II, the fusion threshold energy B_0 deduced from the mean-field transport theories using the technique described in Ref. [41] is

TABLE II. Fusion barrier B_0 (in MeV) for the reaction ^{40}Ca + ^{4x}Ca. Experimental barriers are taken from [42]; theoretical barriers are computed with a precision of 0.005 MeV.

System	B_0 (Exp.)	B_0 (Filling) (MeV)	B_0 (BCS) (MeV)
^{40}Ca + ^{40}Ca	53.6	53.090	53.090
^{40}Ca + ^{42}Ca		52.735	52.735
^{40}Ca + ^{44}Ca	51.8	52.343	52.332
^{40}Ca + ^{46}Ca		52.069	52.049
^{40}Ca + ^{48}Ca	51.8	51.935	51.935
^{40}Ca + ^{50}Ca		51.200	51.247

systematically reported for the different reactions considered here. When available, experimental fusion barriers are also shown. It is clear from the table that the introduction of pairing has a very weak influence on the barrier height.

A. Systematic study of two-particle transfer versus one-particle transfer

In Fig. 7, one- and two-particle transfer probabilities obtained for the collision between calcium isotopes are displayed as a function of center-of-mass energy for the TDHF + BCS case and no-pairing case. In all cases, when one of the collision partners presents pairing, the two-particle transfer probabilities are significantly enhanced. Conjointly, the one-particle transfer is also increased but to a lesser extent. This implies that the mean number of particles exchanged

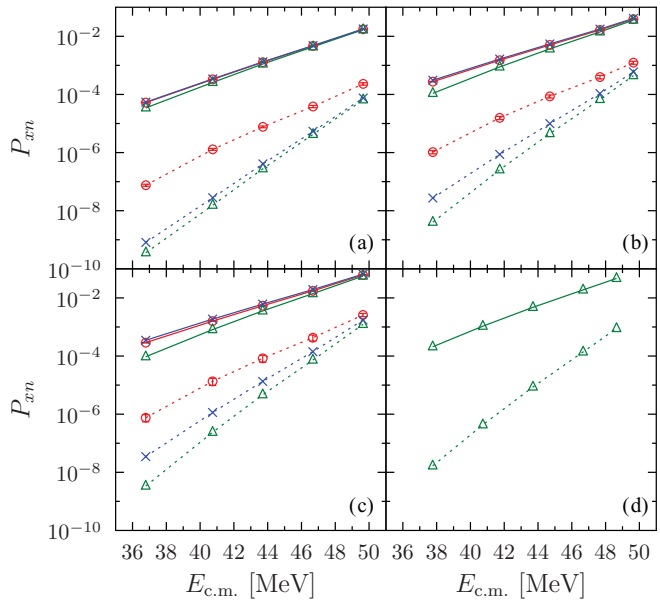

FIG. 7. (Color online) One- (solid line) and two-particle (dashed line) transfer probabilities as a function of center-of-mass energy for the reactions (a) ^{40}Ca + ^{42}Ca, (b) ^{40}Ca + ^{44}Ca, (c) ^{40}Ca + ^{46}Ca, and (d) ^{40}Ca + ^{48}Ca. The TDHF + BCS results obtained by neglecting (crosses) or not (open circles) the anomalous density contribution are systematically compared with the mean-field case (open triangles). Note that for panel (d), both nuclei are closed-shell nuclei and pairing correlations vanish. Accordingly, only the mean-field result is shown.

is also influenced by the pairing correlations owing to the sum rule [Eq. (18)]. Comparing the TDHF results where the effect of κ is included (direct + sequential process) to those of case where it is neglected (sequential only), several conclusions can be drawn. First, the one-particle probability is almost unchanged. Therefore, the enhancement in P_{1n} observed in BCS theory compared to the pure mean-field case is a direct consequence of the specific fragmentation of occupation numbers owing to pairing that reduces Pauli blocking effect during the transfer process and is unaffected by the simultaneous component. A second important conclusion is that the main source of enhancement observed in P_{2n} is coming from the initial two-body correlations themselves that lead to direct processes during the collision. This confirms the observation made in Fig. 6.

B. Correlations between two-particle transfer and pairing gap

To further quantify the influence of pairing correlations on the enhancement of two-particle transfer and possible dependence with center-of-mass energy, the ratio $P_{2n}(\mathrm{BCS})/P_{2n}(\mathrm{MF})$ is displayed as a function of the mass of the heaviest nucleus participating to the collision and for two different fixed center-of-mass energies below the Coulomb barrier. For comparison, the neutron mean gap,

$$\Delta_{\rm BCS} = \frac{\sum_{k>0} \kappa_k \Delta_k}{\sum_{k>0} \kappa_k}, \tag{23}$$

obtained for this nucleus is also shown in panel (a).

Similar to the pairing gap, this ratio has a typical bell shape that drops down to one in magic nuclei (see Fig. 8). This confirms that the enhancement of pair transfer is directly proportional to the initial pairing correlations (see, for instance, the discussion in Ref. [43]).

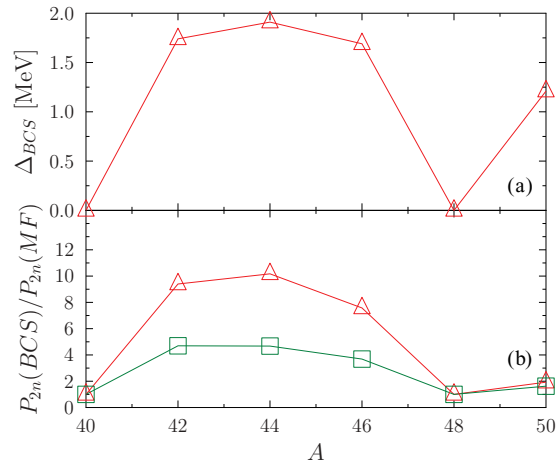

FIG. 8. (Color online) (a) Mean neutron pairing gap obtained with BCS theory for the mixed interaction as a function of mass along the isotopic chain. (b) Ratio of the two-particle transfer probability obtained with and without pairing at fixed center-of-mass energy below the Coulomb barrier reported in Table II. Open squares and open triangles correspond to 4 and 6 MeV below the Coulomb barrier, respectively.

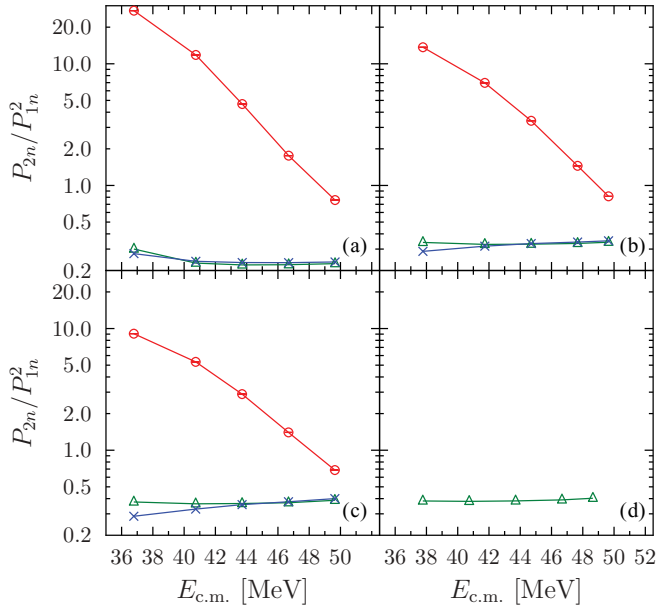

FIG. 9. (Color online) Ratio $P_{2n}/(P_{1n})^2$ as a function of beam energies. The different panels correspond to different reactions: (a) ^{40}Ca + ^{42}Ca, (b) ^{40}Ca + ^{44}Ca, (c) ^{40}Ca + ^{46}Ca, and (d) ^{40}Ca + ^{48}Ca. The TDHF + BCS results obtained by neglecting (crosses) or not (open circles) the anomalous density contribution are systematically compared with the mean-field case (open triangles).

C. Relationship between P_{2n} and P_{1n}^2

Experimentally, the no-pairing limit that would be a reference for a given reaction cannot be measured. It is therefore important to compare quantities that could be measured simultaneously. Usually, the two-particle transfer P_{2n} is compared to $(P_{1n})^2$, where the latter quantity is considered as the probability for a completely sequential transfer [7,8,44]. Such a comparison has the advantage that both quantities contain all possible effects that might influence the transfer of particles as well as possible pollution from coming from experimental setups. In Fig. 9, this ratio is presented for different theories considered here.

This figure gives interesting insight in the two-particle transfer. First, both mean-field and TDHF + BCS where only the fragmentation of single-particle state is accounted for while $C_{12} = 0$, lead to almost identical ratios. This aspect was not clear from Fig. 7, where different fragmentations obtained with the filling approximation and from BCS with $C_{12} = 0$ lead to differences for both P_{1n} and P_{2n}. The mean-field theory or equivalently the BCS where initial correlations are neglected could be considered as a way to mimic independent transfer of the two particles.

It turns out that simple combinatorial arguments can be used to understand analytically the sequential limit. Let us denote by p the average probability to transfer one particle from the ^{4x}Ca to the ^{40}Ca. Here "average" means that we disregard the fact the the probability depends on the initial and final single-particle states. It turns out that the total probability to transfer $1, 2, \ldots, k$ nucleons during the reaction ^{4x}Ca + ^{40}Ca

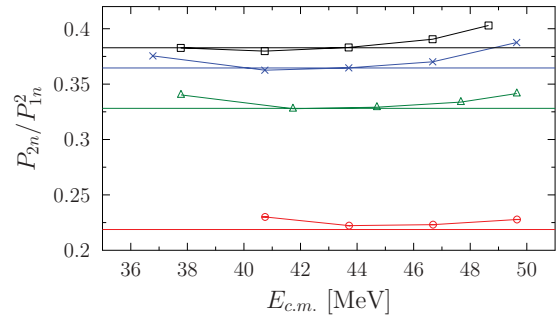

FIG. 10. (Color online) Ratio $P_{2n}/(P_{1n})^2$ as a function of center-of-mass energy for the reaction ^{42}Ca + ^{40}Ca (open circles), ^{44}Ca + ^{40}Ca (open triangles), ^{46}Ca + ^{40}Ca (cross), and ^{48}Ca + ^{40}Ca (open squares). The horizontal lines correspond in each case to the value of the left side of Eq. (25), where $N_f = 8$, while $N_v = x$ for ^{4x}Ca + ^{40}Ca reactions.

for $x > 2$ in the MF approximation is consistent with

$$\begin{aligned} P_{1n} &= \Omega_{1n}\, p(1-p)^{N_v-1}, \\ P_{2n} &= \Omega_{2n}\, p^2(1-p)^{N_v-2}, \\ &\ldots, \\ P_{kn} &= \Omega_{kn}\, p^k(1-p)^{N_v-k}, \end{aligned} \tag{24}$$

where $N_v = x$ is the number of valence nucleons (with the constraint $k < N_v$) in the emitter with respect to the inert core of ^{40}Ca, while Ω_{kn} is a purely combinatorial factor that depends on the number of nucleons in the valence shell and on the number of available single-particle states in the $f^{7/2}$ empty shell of the receiver nucleus ($N_f = 8$). Ω_{kn} simply counts the number of possibilities to select k particles among N_v times the number of ways to put them in the $f^{7/2}$ shell, i.e.,

$$\Omega_{kn} = \frac{N_v!}{k!(N_v-k)!} \times N_f(N_f-1)\cdots(N_f-k+1).$$

Accordingly, one can anticipate that

$$\begin{aligned} \frac{P_{2n}}{(P_{1n})^2} &= \frac{1}{2}\frac{(N_v-1)}{N_v}\frac{(N_f-1)}{N_f} \times \frac{1}{(1-p)^{N_v}} \\ &\simeq \frac{1}{2}\frac{(N_v-1)}{N_v}\frac{(N_f-1)}{N_f}, \end{aligned} \tag{25}$$

where the last approximation holds if $p \ll 1$.

This simple approximation turns out to work very well in the mean-field case (or equivalently in the pairing case when κ is neglected). In Fig. 10, the quantity $P_{2n}/(P_{1n})^2$ is compared to the left side of Eq. (25) for the different reactions considered here. We see that for a wide range of center-of-mass energy, mean-field results perfectly match the relation (25). The fact that such a simple description is adequate in mean-field theory is not trivial. Indeed, in this theory, nucleons are quantal objects interacting first with two cores (the emitter and the receiver nucleus) that are not fully inert and second with each other through the self-consistent mean field. Last, the two transferred nuclei are fermions and are subject to the Pauli exclusion principle. This induces automatically correlations during the transfer. If a particle is already transferred to a certain single-particle level, this automatically forbids the

other particles to be transferred to the same level. The latter effect is automatically included in the present theory and partially described through the factor Ω_{kn} in Eq. (24).

Focusing now on the results accounting for initial correlations (open circles in Fig. 9), a strong, center-of-mass energy-dependent enhancement of the ratio is seen. The ratio increases significantly as the energy decreases from a value lower than 1 up to 20 in some cases. The present enhancement is at variance with the recent experimental observation in ^{40}Ca + ^{96}Zr where $P_{2n} \simeq 3(P_{1n})^2$ has been observed almost independently of the center-of-mass energy [7]. It is worth mentioning, however, that the one- and two-particle transfer is anticipated to depend significantly on the structure properties, single-particle energies, and spectroscopic factors of the two collision partners.

In addition, here we are focusing on pairing correlation effect and pay particular attention to not mixing effects coming from static deformation in nuclei. Last, mean field alone cannot grasp the physics of the quantum fluctuations in collective space. The inclusion of pairing partially cures this problem by increasing fluctuations of two-body observables. However, pairing alone does not contain all physical effects to treat this problem. This is clearly illustrated close to magicity where pairing vanishes. In that case, TDHF dynamics is known to fail to reproduce transfer cross section. Recently, a stochastic mean-field approach was shown to properly describe quantal collective fluctuations, especially in magic nuclei [45–48] and leads to realistic description of the nucleon exchange process. It would be interesting, in the near future, to explore the possibility to combine stochastic methods with the present BCS approach.

IV. CONCLUSION

The TDHF + BCS theory with frozen correlations is used here to investigate the effect of pairing on one- and two-nucleon transfer below the Coulomb barrier. A method based on projection onto particle number is developed to properly extract transfer probabilities from theories that break the U(1) symmetry. In addition, particular attention is paid to compare with a no-pairing limit free from possible effects of deformation. With this technique, the enhancement of two-particle transfer owing to pairing correlations is studied qualitatively and quantitatively for reactions involving different calcium isotopes. It is shown that when one of the collision partners has nonzero pairing, a strong enhancement of pair transfer is observed. This increase is directly proportional to the initial pairing correlations in the superfluid nucleus and turns out to depend strongly on the center-of-mass energy.

ACKNOWLEDGMENTS

We would like to thank G. Adamian, G. Antonenko, S. Kalandarov, G. Bertsch, D. Gambacurta, M. Grasso, V. Sargsyan, C. Simenel, and K. Washiyama for helpful discussions.

APPENDIX: FORMULAS FOR PROJECTION

In the present appendix, formulas useful for the numerical estimate of particle number projection are given for many-body quasiparticle states and density operators respectively given by Eqs. (3) and (22).

1. Particle number projection of density operators

Starting from the density (22), the probability to have N particles in the subspace B can be written as

$$P_B(N) = \frac{1}{2\pi}\int_0^{2\pi} d\varphi e^{-i\varphi N}\mathrm{Tr}(e^{i\varphi \hat{N}_B}\hat{D}). \tag{A1}$$

The estimate of the trace can be made by writing the operator $\hat{N}_B$ in the canonical basis $\{\varphi_i\}$ associated with the density. Using the expression of $\hat{N}_B$ and the fact that the canonical basis forms a complete basis of the total single-particle space, it could be easily shown that

$$P_B(N) = \frac{1}{2\pi}\int_0^{2\pi} d\varphi e^{-i\varphi N}\mathrm{Tr}(e^{i\varphi \sum_{ij} O^B_{ij} a_i^\dagger a_j}\hat{D}), \tag{A2}$$

where

$$O^B_{ij} \equiv \sum_\sigma \int d\mathbf{r}\varphi_i^*(\mathbf{r},\sigma)\varphi_j(\mathbf{r},\sigma)\Theta(\mathbf{r}) = \langle i|j\rangle_B. \tag{A3}$$

Then, using formula (A.16) of Ref. [49] leads to

$$\begin{aligned}\mathrm{Tr}(e^{i\varphi\hat{N}_B}\hat{D}) &= \frac{1}{z}\exp[\mathrm{Tr}\ln(1+e^{-i\varphi O^B}e^{-M})] \\ &= \frac{1}{z}\det(1+e^{-i\varphi O^B}e^{-M}),\end{aligned} \tag{A4}$$

where

$$\left(e^{-i\varphi O^B}\right)_{ij} = F_{ij}(\varphi) = \delta_{ij} + \langle i|j\rangle_B(e^{i\varphi}-1), \tag{A5}$$

while from formula (8.11) of Ref. [49] we have

$$(e^{-M})_{ij} = \delta_{ij}\frac{n_i}{1-n_i} \tag{A6}$$

and $z = \prod_i(1+\frac{n_i}{1-n_i})$. Altogether, we obtain

$$P_B(N) = \frac{1}{2\pi}\int_0^{2\pi} d\varphi e^{-i\varphi N}\det[(1-n_j)\delta_{ij} + F_{ij}(\varphi)n_j].$$

Note that in the case where the statistical density identifies with a Slater determinant ($n_i = 0, 1$), the formula given in Ref. [38] is properly recovered. Formulas for the double-projection technique can be derived using a similar technique.

2. Projection with quasiparticle states

To perform projection of quasiparticle vacuum onto good particle number, we used the recently proposed Pfaffian method [40,50,51]. Because the Pfaffian technique has been largely discussed recently, here only specific formulas useful

in the present article are given. Again, we first consider the projection on the B subspace as an illustration. We need to perform the overlap between the quasiparticle state (3) and its gauge angle rotated counterpart:

$$|\Psi\rangle = \prod_{k>0}(u_k + v_k a_k^\dagger a_{\bar{k}}^\dagger)|-\rangle,$$
$$|\Psi_B(\varphi)\rangle = \prod_{k>0}(u_k + v_k b_k^\dagger(\varphi) b_{\bar{k}}^\dagger(\varphi))|-\rangle,$$

where

$$b_i^\dagger(\varphi) = \sum_\sigma \int d\mathbf{r} e^{i\varphi\Theta(\mathbf{r})}\varphi_i(\mathbf{r},\sigma)\Psi_\sigma^\dagger(\mathbf{r}), \quad \text{(A7)}$$
$$= \sum_j F_{ij}(\varphi) a_j^\dagger. \quad \text{(A8)}$$

The matrix $\mathbf{F}$ plays the role of the matrix $\mathbf{R}$ in Ref. [40] and the overlap between the nonrotated and rotated state are given by Eq. (5) of this reference. In the present case, we obtain

$$\langle\Psi_0|\Psi_B(\varphi)\rangle = \frac{(-1)^n}{\prod_\alpha^n v_\alpha^2}\mathrm{pf}\begin{bmatrix}\mathcal{K} & \mathcal{M}(\varphi)\\ -\mathcal{M}^t(\varphi) & -\mathcal{K}^*\end{bmatrix},$$

where $\mathcal{K}$ and $\mathcal{M}$ are matrix of size $2n \times 2n$ where n is the number of single-particle states with $i > 0$. These matrices can be decomposed in 2×2 matrix blocks as

$$\mathcal{K} = \begin{bmatrix}\mathbf{0} & [\kappa_{i\bar{i}}\delta_{ij}]\\ -[\kappa_{i\bar{i}}\delta_{ij}] & \mathbf{0}\end{bmatrix}$$

and

$$\mathcal{M}(\varphi) = \begin{bmatrix}[v_i v_j F_{ij}^*(\varphi)] & [v_i v_{\bar{j}} F_{i\bar{j}}^*(\varphi)]\\ [v_{\bar{i}} v_j F_{\bar{i}j}^*(\varphi)] & [v_{\bar{i}} v_{\bar{j}} F_{\bar{i}\bar{j}}^*(\varphi)]\end{bmatrix},$$

where matrix elements are directly indicated in each $n \times n$ block.

For the double projection, the probability to find N' particles in the space B for a system of N particles in the total space is given by

$$P_B(N, N') = \frac{\langle N|\hat{P}_B(N')|N\rangle}{\langle N|N\rangle} = \frac{\langle\Psi|\hat{P}_B(N')\hat{P}(N)|\Psi\rangle}{\langle\Psi|\hat{P}(N)|\Psi\rangle}. \quad \text{(A9)}$$

Therefore, we need to integrate with respect to two gauge angles,

$$\langle\Psi|\hat{P}_B(N')\hat{P}(N)|\Psi\rangle = \frac{1}{4\pi^2}\int_0^{2\pi} d\varphi \int_0^{2\pi} d\varphi' e^{-i\varphi N - \varphi' N'}\langle\Psi|\Psi_B(\varphi,\varphi')\rangle,$$

where $\langle\Psi|\Psi_B(\varphi,\varphi')\rangle$ can be calculated using formula (A9) except that $F_{ij}(\varphi)$ is now replaced by $F_{ij}(\varphi,\varphi') = e^{i\varphi}F_{ij}(\varphi')$.

Numerically, the gauge integrals are discretized using the Fomenko method [52] with 20 points. Note that during the time evolution, owing to accumulated numerical errors, a small violation of orthonormalization between single-particle states can occur; this might lead to large errors in the extracted transfer probabilities. To avoid this problem, a Gram-Schmidt orthonormalization algorithm is used prior to applying the Pfaffian formula.

[1] C. L. Jiang, B. B. Back, H. Esbensen, R. V. F. Janssens, and K. E. Rehm, Phys. Rev. C **73**, 014613 (2006).
[2] S. Misicu and H. Esbensen, Phys. Rev. Lett. **96**, 112701 (2006); Phys. Rev. C **75**, 034606 (2007).
[3] T. Ichikawa, K. Hagino, and A. Iwamoto, Phys. Rev. C **75**, 057603 (2007); Phys. Rev. Lett. **103**, 202701 (2009).
[4] V. V. Sargsyan, G. G. Adamian, N. V. Antonenko, W. Scheid, and H. Q. Zhang, Phys. Rev. C **86**, 014602 (2012).
[5] V. V. Sargsyan, G. G. Adamian, N. V. Antonenko, W. Scheid, and H. Q. Zhang, Phys. Rev. C **85**, 024616 (2012).
[6] A. Lemasson *et al.*, Phys. Rev. Lett. **103**, 232701 (2009).
[7] L. Corradi *et al.*, Phys. Rev. C **84**, 034603 (2011).
[8] W. von Oertzen and A. Vitturi, Rep. Prog. Phys. **64**, 1247 (2001).
[9] G. Ripka and R. Padjen, Nucl. Phys. A **132**, 489 (1969).
[10] D. R. Bès and R. A. Broglia, Nucl. Phys. **80**, 289 (1966).
[11] R. A. Broglia and C. Riedel, Nucl. Phys. A **107**, 1 (1968).
[12] R. A. Broglia, O. Hansen, and C. Riedel, Adv. Nucl. Phys. **6**, 287 (1973).
[13] J. Dobaczewski, W. Nazarewicz, T. R. Werner, J. F. Berger, C. R. Chinn, and J. Decharge, Phys. Rev. C **53**, 2809 (1996).
[14] E. Khan, N. Sandulescu, N. V. Giai, and M. Grasso, Phys. Rev. C **69**, 014314 (2004).
[15] B. Avez, C. Simenel, and Ph. Chomaz, Phys. Rev. C **78**, 044318 (2008).
[16] G. Potel, A. Idini, F. Barranco, E. Vigezzi, and R. A. Broglia, arXiv:0906.4298v3 [nucl-th].
[17] E. Khan, M. Grasso, and J. Margueron, Phys. Rev. C **80**, 044328 (2009).
[18] B. Mouginot *et al.*, Phys. Rev. C **83**, 037302 (2011).
[19] H. Shimoyama and M. Matsuo, Phys. Rev. C **84**, 044317 (2011).
[20] G. Potel, F. Barranco, F. Marini, A. Idini, E. Vigezzi, and R. A. Broglia, Phys. Rev. Lett. **107**, 092501 (2011).
[21] E. Pllumbi, M. Grasso, D. Beaumel, E. Khan, J. Margueron, and J. van de Wiele, Phys. Rev. C **83**, 034613 (2011).
[22] M. Grasso, D. Lacroix, and A. Vitturi, Phys. Rev. C **85**, 034317 (2012).
[23] D. Gambacurta and D. Lacroix, Phys. Rev. C **86**, 064320 (2012).
[24] I. Stetcu, A. Bulgac, P. Magierski, and K. J. Roche, Phys. Rev. C **84**, 051309(R) (2011).
[25] Y. Hashimoto and K. Nodeki, arXiv:0707.3083.
[26] J. Blocki and H. Flocard, Nucl. Phys. A **273**, 45 (1976).
[27] S. Ebata, T. Nakatsukasa, T. Inakura, K. Yoshida, Y. Hashimoto, and K. Yabana, Phys. Rev. C **82**, 034306 (2010).
[28] G. Scamps, Denis Lacroix, G. F. Bertsch, and K. Washiyama, Phys. Rev. C **85**, 034328 (2012).
[29] S. Ebata, arXiv:1211.6812 [nucl-th].

[30] C. Simenel, D. Lacroix, and B. Avez, *Quantum Many-body Dynamics: Applications to Nuclear Reactions* (VDM Verlag, Sarrebruck, Germany, 2010).
[31] K.-H. Kim, T. Otsuka, and P. Bonche, J. Phys. G **23**, 1267 (1997).
[32] P. Bonche, H. Flocard, and P.-H. Heenen, Comput. Phys. Commun. **171**, 49 (2005).
[33] M. Bender, P.-H. Heenen, and P.-G. Reinhard, Rev. Mod. Phys. **75**, 121 (2003).
[34] T. Duguet, P. Bonche, P.-H. Heenen, and J. Meyer, Phys. Rev. C **65**, 014310 (2001).
[35] G. F. Bertsch, C. A. Bertulani, W. Nazarewicz, N. Schunck, and M. V. Stoitsov, Phys. Rev. C **79**, 034306 (2009).
[36] M. Assié and D. Lacroix, Phys. Rev. Lett. **102**, 202501 (2009).
[37] G. Scamps and D. Lacroix (unpublished).
[38] C. Simenel, Phys. Rev. Lett. **105**, 192701 (2010).
[39] C. H. Dasso, T. Dössing, and H. C. Pauli, Z. Phys. A **289**, 395 (1979).
[40] G. F. Bertsch and L. M. Robledo, Phys. Rev. Lett. **108**, 042505 (2012).
[41] C. Simenel and B. Avez, Int. J. Mod. Phys. E **17**, 31 (2008).
[42] K. Siwek-Wilczynska and J. Wilczynski, Phys. Rev. C **69**, 024611 (2004).
[43] D. M. Brink and R. A. Broglia, *Nuclear Superfluidity: Pairing in Finite Systems* (Cambridge University Press, Cambridge, UK, 2005).
[44] L. Corradi, G. Pollarolo, and S. Szilner, J. Phys. G **36**, 113101 (2009).
[45] S. Ayik, Phys. Lett. B **658**, 174 (2008).
[46] S. Ayik, K. Washiyama, and D. Lacroix, Phys. Rev. C **79**, 054606 (2009).
[47] K. Washiyama, S. Ayik, and D. Lacroix, Phys. Rev. C **80**, 031602(R) (2009).
[48] B. Yilmaz, S. Ayik, D. Lacroix, and K. Washiyama, Phys. Rev. C **83**, 064615 (2011).
[49] R. Balian and M. Veneroni, Ann. Phys. **164**, 334 (1985).
[50] L. M. Robledo, Phys. Rev. C **79**, 021302 (2009).
[51] B. Avez and M. Bender, Phys. Rev. C **85**, 034325 (2012).
[52] V. N. Fomenko, J. Phys. G **3**, 8 (1970).